ORIGINAL PAPER

Macroscopic Auxetic Materials and Models

physica status solidi b

www.pss-b.com

Flexible Cube Tilt Lattice with Anisotropic Cosserat Effects and Negative Poisson's Ratio

*Zach Rueger, Chan Soo Ha, and Roderic S. Lakes**

A 3D lattice structure consisting of pivoting cubes with flexible links at the corners is presented. It exhibits anisotropic negative Poisson's ratio −0.54 and −0.75. Size effects occur in torsion and bending; these effects are consistent with Cosserat elasticity but not with classical elasticity. Cosserat elastic solids exhibit sensitivity to strain gradients; size effects occur in torsion and bending; also reduction in stress concentrations. The observed Cosserat effects also reveal anisotropy.

1. Introduction

Negative Poisson's ratio materials are by now well known. A 3D isotropic negative Poisson's ratio material based on transformed open cell polyurethane foam was reported[1] in 1987; it had a Poisson's ratio −0.7; metal foams of similar structure can have Poisson's ratio as small as −0.8.[2] Negative Poisson's ratio materials have been called "dilational"[3] because they easily undergo volume changes but are difficult to shear. An ideal dilational material would approach the isotropic lower limit on Poisson's ratio −1. Hierarchical two phase composites were developed and studied; Poisson's ratio approaches −1 as contrast between constituent moduli is increased. A 2D honeycomb with inverted hexagonal cells[4] can exhibit negative Poisson's ratio; a 2D chiral lattice[5] exhibits a Poisson's ratio of −1 over a range of strain as shown by experiment and analysis.

Hinged structures are of interest in part because they can be readily shown to exhibit negative Poisson's ratio, and in part because with the advent of 3D printing, one can seek to approximate such lattices in physical form. Structures of hinged polygons, called hinged tessellations, have been studied from the perspective of mathematics[6–8] rather than physical properties. These are the earliest known hinged polygon constructions. A Poisson's ratio of −1 can be attained via inverse homogenization in 2D structures with rotating rigid squares connected at the corners by ideal hinges.[9] Rotating squares were considered[10] as a model for the negative Poisson's ratio in some crystals. Rotating hinged squares were developed independently to achieve a Poisson's ratio −1.[11] Related 2D systems with rotating hexamers;[12,13] rotating rhombi,[14] triangles,[15] and prisms,[16] also give rise to negative Poisson's ratio. Related structures with hinged components can exhibit negative Poisson's ratio and zero bulk modulus, with arbitrarily large volumetric strain.[17]

It had been suggested in view of the original foams that a coarse cell structure is needed to control the Poisson's ratio[18] and that moments carried by the structural elements constitute a hidden state variable that gives rise to a negative Poisson's ratio. Indeed many such materials do have cells of large size. However theories that incorporate distributed moments, as presented below, allow the same range of Poisson's ratio as in classical elasticity.[19] Negative Poisson's ratio is known to occur in materials in the vicinity of a phase transformation. These materials have fine scale structure; they constitute a counterexample to the suggestion that a coarse structure is necessary. Further details on causes of negative Poisson's ratio are provided elsewhere.[20]

A 3D structure of cubes connected by ideal hinges or pivots was found to exhibit anisotropic negative Poisson's ratio.[21] It is also of interest because it does not obey classical elasticity. Stretching of the lattice causes tilting of the cubes at the hinges. Void space appears in the structure so there is a volume change. The structure expands laterally under tension so there is a negative Poisson's ratio. The symmetry at first sight appears to be cubic; orthotropic anisotropy arises from the connectivity of the hinges. Young's modulus is zero but Poisson's ratio depends on direction. If the hinges are ideal, the structure has zero resistance to axial stretching but is rigid with respect to torsion and bending. In a classical solid, the same Young's modulus that governs tension must also apply to bending. Classical elasticity is insensitive to gradients in strain such as those in bending. Such extreme sensitivity to strain gradients may be interpreted in the context of Cosserat elasticity, a generalized continuum theory of elasticity which allows sensitivity to strain gradients.

The Cosserat theory of elasticity[22,23] is a *continuum* theory that incorporates local rotation of points as well as displacement of points. Micropolar elasticity[24] incorporates an inertia term that affects wave propagation. The stress σ_{ij} (force per unit area) can be asymmetric. The resulting distributed moment from this asymmetry is balanced by a couple stress m_{ij} (a torque per unit area). The antisymmetric part of the stress is related to rotations colorblue of points: $\sigma_{ij}^{\text{antisym}} = \kappa e_{ijk}\left(r_k - \phi_k\right)$ in which κ is an elastic constant, ϕ_k is the rotation of points, called micro-rotation, e_{ijk} is the permutation symbol, and $r_k = \frac{1}{2} e_{klm} u_{ml}$ is "macro" rotation based on the antisymmetric part of gradient of

Dr. Z. Rueger, Dr. C. S. Ha, Prof. R. S. Lakes
Department of Engineering Physics
Department of Materials Science
University of Wisconsin
Madison, WI 53706-1687, USA
E-mail: rlakes@wisc.edu

DOI: 10.1002/pssb.201800512

displacement u_i. The constitutive equations[24] for linear isotropic Cosserat elasticity are:

$$\sigma_{ij} = 2G\varepsilon_{ij} + \lambda\varepsilon_{kk}\delta_{ij} + \kappa e_{ijk}\left(r_k - \phi_k\right) \tag{1}$$

$$m_{ij} = a\phi_{k,k}\delta_{ij} + \beta\phi_{i,j} + \gamma\phi_{j,i} \tag{2}$$

The usual Einstein summation convention for repeated indices is used. The comma indicates partial differentiation. The six isotropic Cosserat elastic constants are expressed as the following technical constants which are helpful for physical insight. Here, λ is a Lamé constant from elasticity theory. The range of Poisson's ratio is the same in Cosserat solids as in classical solids.

$$\text{Young's modulus} \quad E = \frac{G(3\lambda + 2G)}{\lambda + G} \tag{3}$$

$$\text{Shear modulus} \quad G \tag{4}$$

$$\text{Poisson's ratio} \quad \nu = \frac{\lambda}{2(\lambda + G)} \tag{5}$$

$$\text{Characteristic length, torsion} \quad \ell_t = \sqrt{\frac{\beta + \gamma}{2G}} \tag{6}$$

$$\text{Characteristic length, bending} \quad \ell_b = \sqrt{\frac{\gamma}{4G}} \tag{7}$$

$$\text{Coupling number} \quad N = \sqrt{\frac{\kappa}{2G + \kappa}} \tag{8}$$

$$\text{Polar ratio} \quad \Psi = \frac{\beta + \gamma}{a + \beta + \gamma} \tag{9}$$

Specific nonclassical effects include size effects in which slender bars in torsion[25] or bending appear to have higher moduli than thicker ones, and reduction in the concentration of stress or strain around holes or other heterogeneities.

The characteristic lengths govern the size scale at which nonclassical effects may be expected. The coupling number governs the magnitude of the effects.

If the material is anisotropic, these constants can be interpreted as technical constants with direction dependence as is done in classical elasticity. Specifically, one can determine Young's modulus E and Poisson's ratio ν in different directions without using the classical tensorial constants C_{ijkl}. Similarly in the Cosserat case one can infer constants based on measurements with strain gradients in different directions.

Cosserat elastic constants can be determined from size dependence of rigidity in torsion and bending.[25] Such experiments disclosed purely classical behavior in aluminum[26] and also in a particulate composite containing aluminum beads in an epoxy matrix.[25] Cosserat effects were observed in a dense closed cell foam[27] and in low density negative Poisson's ratio foam.[28] Cosserat effects were observed in in a two-dimensional circular cell polymer honeycomb[29] and in a 2D lattice[30] originally developed to exhibit chirality and a Poisson's ratio −1.[5] Strong Cosserat effects were observed in a lattice[31] designed to manifest such behavior.

Structures with ideal hinges are of conceptual interest but they are not so easy to fabricate. In particular they cannot be made by 3D printing. In the present study, we fabricate and study a flexible structure made of cubes connected by deformable links at their corners. This structure is similar in geometry to a hinged lattice studied theoretically;[21] the deformable links are non-ideal hinges. In the present research, Poisson's ratio and sensitivity to gradients are determined experimentally for the flexible cube structure.

2. Experimental Section

The lattice structure (Figure 1) is comprised of cubes of side length $a = 6$ mm connected by flexible links 1 mm long at the corners. Figure 2 shows the detailed structure of the link elements. Preliminary trials were done using different link lengths. The thickness of the links was limited by the resolution of the 3D printer. The cubes were provided with a slight tilt to prevent contact between them during compression. The lattices

Figure 1. Lattice structure, oblique view. Scale bar, foreground, 10 mm.

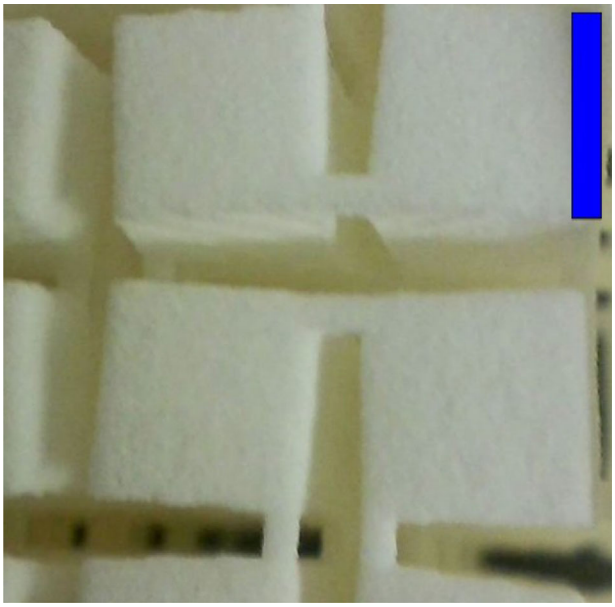

Figure 2. Lattice structure, close up view. Scale bar, 5 mm.

were physically embodied using a 3D Systems sPro 60 HS-HD selective laser sintering 3D printer. The parent material was a polyamide stated to be equivalent to nylon 12. Lattices of different size were made to enable size effect measurements. Each lattice was cemented to metal end pieces to provide appropriate end conditions. The specimen length was three times the width. That aspect ratio was considered sufficient to minimize end effects according to Saint Venant's principle. Indeed,[32] if Poisson's ratio is not extreme, an aspect ratio of one to one suffices to limit the error to about 3%. The width in the transverse directions was the same. In any case, use of the same aspect ratio for each size specimen implies the role of end effects is independent of specimen size. The longitudinal axis is defined as a center line in the long direction of the specimen.

Specimens were 3, 4, 6, and 8 cubes in width. A specimen 10 cubes in width was also made but difficulties in the 3D printing process rendered it unusable. Due to the connectivity of the alternating link structure, specimens fewer than 3 cubes in width did not have sufficient mechanical integrity to be included.

Compression tests were done to determine Young's modulus in the absence of imposed gradients. Poisson's ratio was determined from compression testing by measuring transverse deformation via digital photography and via a micrometer.

Torsional and bending rigidities for each specimen were measured using broadband viscoelastic spectrometry (BVS). The BVS makes use of a pair of orthogonal Helmholtz coils to generate a torque upon a magnet at the free end. Bending or torsion can be achieved depending on which coil is excited by an electric current of known magnitude. The method allows torsion and pure bending tests to be conducted on the same specimen. The magnetic field acts upon a high intensity permanent magnet attached to the specimen's end piece via a ceramic stalk. The torque M is given by the cross product $M = \mu \times B$ in which μ is the magnetization vector of the magnet and B is the magnetic field imposed by the Helmholtz coil. Torque was calculated from the voltage across a 1 Ω resistor in series with each coil. Torque sensitivity was calibrated via measurements on the well characterized 6061 aluminum alloy.

Deformation of each specimen was measured from motion of a laser beam reflected from a mirror cemented to the magnet attached to the bottom of the specimen or to the bottom end piece of each specimen. colorblue The top end was fixed. Mounting mirrors on the end piece was done for the larger specimens to eliminate possible error from compliance of the ceramic stalk. A position sensitive silicon light detector was used to convert either horizontal or vertical displacement of the laser beam to a change in voltage. Vertical displacements correspond to bending and horizontal displacements correspond to torsion. The light detector was calibrated via motion from precision vertical and horizontal translation stages.

The input signal was a sinusoidal signal with a frequency of 1 Hz from an SRS Model DS345 function generator. A frequency of 1 Hz is well below any resonant frequencies so a quasi-static interpretation is appropriate. The same frequency was used for all tests, so viscoelastic effects are decoupled from size effects.

2.1. Analysis and Interpretation

Simple compression, in which there are no imposed gradients, reveals Young's modulus E and Poisson's ratio ν. For analyzing and interpreting torsion and bending data, analytical solutions for square cross sections of isotropic Cosserat solids were used. Size effects are quantified by Ω as the ratio of structural rigidity to its classical counterpart.

For torsion of a square cross section Cosserat elastic bar of width $2a$, the twisting moment M is as follows, with θ as the angular displacement per length. For a classically elastic solid,

$$M = \frac{898}{399} G a^4 \theta \tag{10}$$

The structural rigidity is $\frac{M}{\theta}$.

For a Cosserat solid when $\kappa \to \infty$, corresponding to $N = 1$, the total torque M[33] simplifies to

$$M = \frac{4}{21} G \left(\frac{a}{2}\right)^4 \theta \frac{1796 + 126\left(449 + 2740\bar{\ell}^2 + 3960\bar{\ell}^4\right)\bar{\ell}^2 + 693\left(152 + 2280\bar{\ell}^2 + 6615\bar{\ell}^4\right)\bar{\ell}_b^2}{8\left(19 + 465\bar{\ell}^2 + 990\bar{\ell}^4\right) + 1485\left(6 + 49\bar{\ell}^2\right)\bar{\ell}_b^2} \tag{11}$$

in which $\bar{\ell} = 2\ell_t/a$, $\bar{\ell}_b = 2\ell_b/a$. The ratio of Cosserat rigidity to classical rigidity is defined as Ω, called the rigidity ratio or relative stiffness. This solution is superior in the regime of strong coupling or for $\beta/\gamma < 0$, to that of ref. [34], which overestimates the effects for large N approaching or equal to 1. In the present experiments the shear modulus G is obtained from the asymptotic rigidity as width becomes large. The

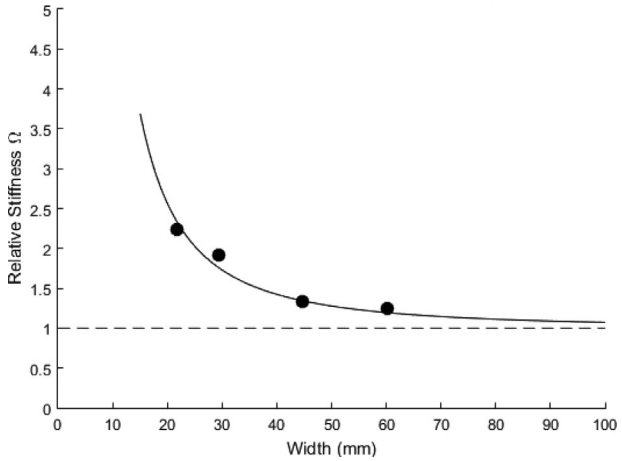

Figure 3. Torsion size effects. The solid curve is theoretical for $G = 2.5$ MPa, $\ell_t = 5.2$ mm, and $N = 1$. Classical elasticity predicts Ω independent of width as illustrated by the horizontal dashed line. The smallest specimen was 3 cubes across; the largest was 8 cubes across, for all tests.

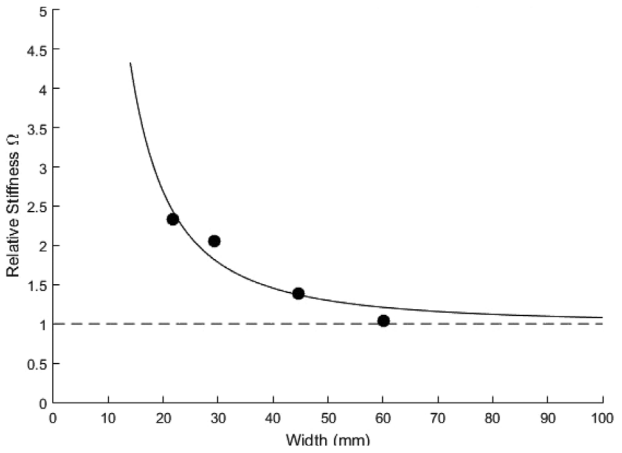

Figure 4. Torsion size effects after 90° rotation about the longitudinal axis. The solid curve is theoretical for $G = 2.4$ MPa, $\ell_t = 5.4$ mm, and $N = 1$. Classical elasticity predicts Ω independent of width as illustrated by the horizontal dashed line.

characteristic length ℓ_t is obtained from the increase in torsion relative stiffness Ω as width becomes small. Equation (11) contains ℓ_b but the rigidity is very weakly dependent on ℓ_b. If $N < 1$ and Ψ is not too far from its upper limit 1.5, the plot of Ω *vs.* width $2a$ levels off for small width. That is not seen in the present experiments. Torsion experiments reveal Ψ only if $N < 1$.

For bending of a rectangular bar of width $2a$, the rigidity ratio (relative stiffness) depends on the bending characteristic length ℓ_b and the Poisson's ratio.[35] If $\beta/\gamma = -\nu$, the rigidity ratio is $\Omega = \frac{M}{1/R}\frac{1}{EI}$, with M as moment, I as moment of inertia of the cross section and R as radius of curvature,

$$\Omega = \left[1 + 24(\ell_b/2a)^2(1-\nu)\right] \tag{12}$$

For arbitrary values of Poisson's ratio, the rigidity ratio is, (to fourth order in $\ell_b/2a$),

$$\Omega = [1 + 24\frac{1 + 2\frac{\beta}{\gamma}\nu + \nu^2}{1+\nu}\left(\frac{\ell_b}{2a}\right)^2 - 480\left(\frac{\beta}{\gamma}_{+\nu}\right)^2\frac{44 - 38\nu + 3N^2(1-\nu)(13-9\nu)}{N^2(1+\nu)(22-19\nu)}\left(\frac{\ell_b}{2a}\right)^4] \tag{13}$$

In the experiments the Young's modulus E and Poisson's ratio ν were obtained obtained from compression tests. The characteristic length ℓ_b was obtained from the increase in bending relative stiffness Ω as width becomes small. N and β/γ were obtained from the detailed shape of the curve.

3. Results and Discussion

The average density for these structures was 0.47 g/cc. Poisson's ratio ν obtained from compression was −0.54 and −0.75 in two orthogonal transverse directions; Young's modulus E in the longitudinal direction was 0.91 MPa. As with the cube structure with ideal hinges,[21] orthotropic anisotropy arises from the connectivity of the flexible hinge-like links.

Results of torsion size effect studies are shown in Figure 3 and 4. The specimen was rotated 90° about its longitudinal axis between these tests. Such a rotation changes the direction of strain gradient in bending but not in torsion. It is entirely distinct from the small rotations, less than 1°, of the free end during testing. There is minimal difference in the elastic constants obtained from the two experiments as is expected: the torque was in the same direction for both and the same strain gradients apply. The goodness of fit was $R^2 = 0.94$ for 0° rotation and $R^2 = 0.91$ for 90° rotation. Curve fits based on Equation (11) involve both ℓ_t and ℓ_b. Because rigidity is strongly dependent on ℓ_t but very weakly dependent on ℓ_b, the value of ℓ_b from the fit is not sufficiently precise to be meaningful.

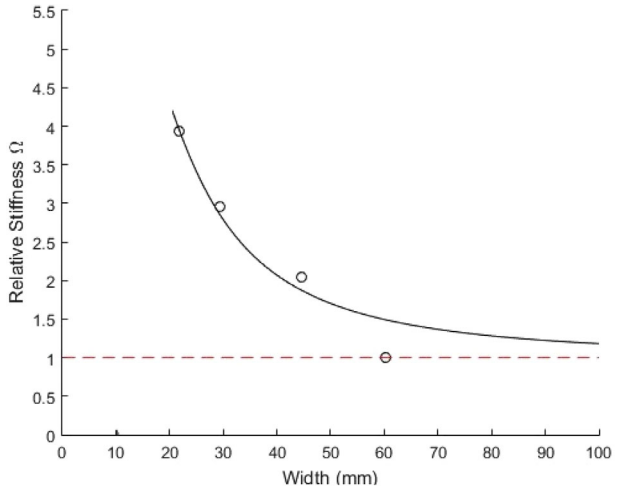

Figure 5. Bending size effects. The solid curve is theoretical for $E = 0.91$ MPa, $\ell_b = 8.5$ mm, and $N = 0.21$; $\beta/\gamma = 0.6$. Classical elasticity predicts $\Omega = 1$ independent of width as illustrated by the horizontal dashed line.

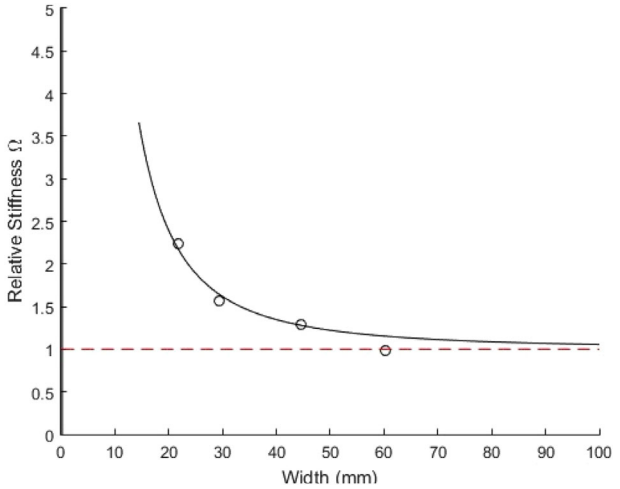

Figure 6. Bending size effects after 90° rotation about the longitudinal axis. The solid curve is theoretical for $E = 0.91$ MPa, $\ell_b = 4.7$ mm, and $N = 0.99$; $\beta/\gamma = 0.8$. Classical elasticity predicts $\Omega = 1$ independent of width as illustrated by the horizontal dashed line.

We remark that an initial value of ℓ_b was input from the bending tests as 8.5 and 4.7 mm, respectively. The fitting for torsion did not alter these initial values.

For bending, rotation of the specimen about its longitudinal axis makes a difference in the pertinent component of deformation gradient as indicated by the difference in Ω and in ℓ_b in Figure 5 and 6. The goodness of fit was $R^2 = 0.94$ for 0° rotation and $R^2 = 0.95$ for 90° rotation about the longitudinal axis. The Young's modulus E was obtained from compression experiments. By contrast to a similar structure with ideal hinges, the Young's modulus does not vanish. The characteristic lengths differ as is expected from the anisotropic nature of the structure. The Cosserat anisotropy differs from classical anisotropy in that for bending, the stress is in the longitudinal direction for both orientations. Only the gradient in stress depends on rotation about the longitudinal axis.

A summary of the elastic constants of the cube structure is as follows. $G = 2.45$ MPa, $\ell_t = 5.3$ mm, and $N = 1$ for torsion; $E = 0.91$ MPa, $\nu_1 = -0.54$, $\nu_2 = -0.75$; $\ell_{b1} = 8.5$ mm, and $N_1 = 0.21$; $\ell_{b2} = 4.7$ mm, and $N_2 = 0.21$. For comparison with the characteristic lengths, the cube width was 6 mm. Because the lattice is anisotropic, one does not expect the isotropic interrelations among the elastic constants to apply.

Bending in the direction shown in Figure 5 revealed the largest magnitude of size effects in this series. By contrast to a similar cube structure with ideal hinges,[21] the present cube structure, which has flexible hinge-like ligaments, does not have a zero value of Young's modulus E in tension/compression. The zero E in the ideal hinged cube structure[21] combined with rigidity in torsion and bending imply Cosserat characteristic lengths that tend to infinity. In the present cube structure the cubes are linked with flexible ligaments that, in contrast with perfect hinges, have a nonzero resistance to rotation; they also have a finite resistance to translation. As a result, the Cosserat effects are of finite magnitude. In a related vein, a 3-D printed material[36] inspired by an ideal structure of hinged rotating squares[11] exhibited a Poisson's ratio of −0.8 in comparison with −1 for the ideal hinged structure.

Cosserat size effects in the present lattice were of modest magnitude compared with those in a prior triangular cell lattice[31] designed for strong effects. The torsional characteristic length, 5.3 mm, is somewhat smaller than the cube width, 6 mm. The maximum torsional size effect, less than a factor of 2.5, was considerably smaller than the factor 35 observed in the triangular cell lattice.[31] One reason is that the present lattice required at least three cubes in the transverse direction of the smallest specimen to provide a unit cell in view of the alternating structure of the ligaments. It is also a different structure. In bending the characteristic length in one direction was larger than in the other but the maximum size effect was less than a factor of 4, again in part as a result of the unit cell size and in part from the structural geometry.

Idealized hinged structures are of interest in part because visualization and analysis are facilitated. Ideal hinges are not so easy to fabricate, particularly in lattices for which many hinges are desired. Flexible hinge-like ligaments resist rotation and have compliance to compression and shear, unlike ideal hinges which freely rotate and are rigid to compression and shear. Flexible ligaments therefore capture only a portion of the intended behavior, both in classical and in Cosserat elasticity.

4. Conclusions

A lattice structure consisting of pivoting cubes with flexible links at the corners is made by 3D printing and studied experimentally. Poisson's ratio is negative and anisotropic. Size effects occur in torsion and bending; these effects are consistent with Cosserat elasticity but not with classical elasticity. The Cosserat effects also reveal anisotropy.

Acknowledgements

Patial support of this research by the National Science Foundation via Grant CMMI-1361832 is acknowledged.

Conflict of Interest

The authors declare no conflict of interest.

Keywords

auxetic, Cosserat, negative Poisson's ratio

Received: September 27, 2018
Revised: October 17, 2018
Published online: November 23, 2018

[1] R. S. Lakes, *Science* **1987**, *235*, 1038.
[2] J. B. Choi, R. S. Lakes, *J. Mater. Sci.* **1992**, *27*, 5373.
[3] G. W. Milton, *J. Mech. Phys. Solids* **1992**, *40*, 1105.
[4] L. J. Gibson, M. F. Ashby, G. S. Schajer, C. I. Robertson, *Proc. Royal Society London* **1982**, *A382*, 25.

[5] D. Prall, R. S. Lakes, *Int. J. Mechanical. Sci*. **1996**, *39*, 305.
[6] D. Stuart, *Polyhedral and Mosaic Transformations*, Vol. 12 (1) Student Publications of the School of Design, Raleigh, North Carolina, USA 1963, pp. 2–28.
[7] D. Wells, *Hidden Connections, Double Meanings*. Cambridge University Press, Cambridge, UK **1988**.
[8] G. N. Frederickson, *Hinged Dissections*. Cambridge University Press, Cambridge, UK **2002**.
[9] O. Sigmund, *Int. J. Solids Struct*. **1994**, *31*, 2313.
[10] Y. Ishibashi, M. Iwata, *J. Phys. Soc. Jpn*. **2000**, *69*, 2702.
[11] J. N. Grima, A. Alderson, K. E. Evans, *Physica Status Solidi B* **2005**, *242*, 561.
[12] K. W. Wojciechowski, *Mol. Phys*. **1987**, *61*, 1247.
[13] K. W. Wojciechowski, *Phys. Lett. A* **1989**, *137*, 60.
[14] D. Attard, J. N. Grima, *Phys. Status Solidi (b)* **2008**, *245*, 2395.
[15] J. N. Grima, K. E. Evans, *J. Mater. Sci*. **2006**, *41*, 3193.
[16] D. Attard, J. N. Grima, *Phys. Status Solidi B* **2012**, *249*, 1330.
[17] G. W. Milton, *J. Mech. Phys. Solids* **2013**, *61*, 1543.
[18] S. Burns, *Science* **1987**, *238*, 551.
[19] R. S. Lakes, *Science* **1987**, *238*, 551.
[20] R. S. Lakes, *J. Mater. Sci*. **1991**, *26*, 2287.
[21] C. Andrade, C. S. Ha, R. S. Lakes, *J. Mech. Mater. Struct*. **2018**, *13*, 93.
[22] E. Cosserat, F. Cosserat, *Theorie des Corps Deformables*. Hermann et Fils, Paris **1909**.
[23] R. D. Mindlin, *Int. J. Solids Struc*. **1965**, *1*, 265.
[24] A. C. Eringen, *Fracture*, Vol. *1*, (Ed: H. Liebowitz), Academic Press, NY **1968**, p. 621.
[25] R. D. Gauthier, W. E. Jahsman, *J. Appl. Mech*. **1975**, *42*, 369.
[26] J. Schijve, *J. Mech. Phys. Solids* **1966**, *14*, 113.
[27] R. S. Lakes, *Int. J. Solids Struct*. **1986**, *22*, 55.
[28] Z. Rueger, R. S. Lakes, *Smart Mater. Struct*. **2016**, *25*, 8pp.
[29] R. Mora, A. M. Waas, *Philos. Mag. A* **2000**, *80*, 1699.
[30] A. Spadoni, M. Ruzzene, *J. Mech. Phys. Solids* **2012**, *60*, 156.
[31] Z. Rueger, R. S. Lakes, *Phys. Rev. Lett*. **2018**, *120*, 065501.
[32] L. N. G. Filon, *Phil. Trans. Royal Soc. Lond. Eng. Ser. A* **1902**, *198*, 147.
[33] W. J. Drugan, R. S. Lakes, *Z. Angew. Math. Phys*. **2018**, *69*, 24.
[34] H. C. Park, R. S. Lakes, *Int. J. Solids Struc*. **1987**, *23*, 485.
[35] R. S. Lakes, W. J. Drugan, *J. Appl. Mech*. **2015**, *82*, 091002.
[36] T. Buckmann, R. Schittny, M. Thiel, M. Kadic, G. W. Milton, M. Wegener, *New J. Phys*. **2014**, *16*, 033032.